

Phytogenic biosynthesis and emission of methyl acetate

KOLBY JARDINE¹, FREDERIK WEGENER^{2,3}, LEIF ABRELL⁴, JOOST VAN HAREN⁵ & CHRISTIANE WERNER²

¹Climate Science Department, Earth Science Division, Lawrence Berkeley National Laboratory, Berkeley, CA 94720, USA, ²AgroEcosystem Research, University of Bayreuth, Universitätsstr. 30, 95447 Bayreuth, Germany, ³Experimental and Systems Ecology, University of Bielefeld, Universitätsstrasse 25, D-33615 Bielefeld, Germany, ⁴Department of Chemistry & Biochemistry, Department of Soil, Water and Environmental Science, and ⁵Biosphere 2, University of Arizona, Tucson, AZ 85721, USA

ABSTRACT

Acetylation of plant metabolites fundamentally changes their volatility, solubility and activity as semiochemicals. Here we present a new technique termed dynamic ¹³C-pulse chasing to track the fate of C₁₋₃ carbon atoms of pyruvate into the biosynthesis and emission of methyl acetate (MA) and CO₂. ¹³C-labelling of MA and CO₂ branch emissions respond within minutes to changes in ¹³C-positionally labelled pyruvate solutions fed through the transpiration stream. Strong ¹³C-labelling of MA emissions occurred only under pyruvate-2-¹³C and pyruvate-2,3-¹³C feeding, but not pyruvate-1-¹³C feeding. In contrast, strong ¹³CO₂ emissions were only observed under pyruvate-1-¹³C feeding. These results demonstrate that MA (and other volatile and non-volatile metabolites) derive from the C_{2,3} atoms of pyruvate while the C₁ atom undergoes decarboxylation. The latter is a non-mitochondrial source of CO₂ in the light generally not considered in studies of CO₂ sources and sinks. Within a tropical rainforest mesocosm, we also observed atmospheric concentrations of MA up to 0.6 ppbv that tracked light and temperature conditions. Moreover, signals partially attributed to MA were observed in ambient air within and above a tropical rainforest in the Amazon. Our study highlights the potential importance of acetyl coenzyme A (CoA) biosynthesis as a source of acetate esters and CO₂ to the atmosphere.

Key-words: acetyl fragment; dynamic pulse chase; methyl acetate; pyruvate positional labelling; secondary metabolism; stable carbon isotopes; volatile organic compound.

INTRODUCTION

Emissions from terrestrial vegetation are the largest source of volatile organic compounds (VOCs) to the atmosphere. These compounds affect a number of important atmospheric processes crucial to air quality and climate, including the production of ground level ozone and secondary organic aerosols (Went 1960; Rasmussen 1972). Although their identities, quantities and biological functions remain uncertain, model estimates suggest that oxygenated VOCs contribute up to 22% of the 10¹⁵ g emitted into the atmosphere annually as biogenic VOCs (Guenther *et al.* 1995, 2012). One group of oxygenated compounds emitted by plants that play important ecological roles, including plant–plant and plant–insect

interactions, are volatile acetate esters (Engelberth *et al.* 2004; Chehab *et al.* 2008, 2010). Volatile acetate esters have particularly pleasant odours and are key aroma compounds in flowers (Shalit *et al.* 2003; Knudsen *et al.* 2004), fruits (Hansen *et al.* 1992; Ueda *et al.* 1992), spices (Herderich *et al.* 2010; Szewczyk, Wolfe & Mencer 2011) and beverages (Ramey & Ough 1980; Wieland *et al.* 2012). An enormous array of volatile acetate esters can be produced and emitted from plants, including short chain acetate esters (e.g. methyl acetate, ethyl acetate) (Suchet *et al.* 2011), medium chain acetate esters (e.g. propyl acetate, butyl acetate, pentyl acetate) (Takeoka, Buttery & Flath 1992), monoterpene acetate esters (e.g. citronellyl acetate, geranyl acetate, bornyl acetate, terpinyl acetate, linalyl acetate) (Yani *et al.* 1993; Mondello *et al.* 1998), aromatic acetate esters (e.g. benzyl acetate, phenyl ethyl acetate) (Dudareva *et al.* 1998; Guterma *et al.* 2006) and fatty acid-derived acetate esters (e.g. Z-3-hexen-1-yl acetate, hexyl acetate) (Fall *et al.* 1999; Jardine *et al.* 2012; Pellegrini *et al.* 2012).

In plants, acetate esters of metabolites and biopolymers normally derive from the transfer of an acetyl moiety from acetyl coenzyme A (acetyl CoA) to an alcoholic substrate catalyzed by an alcohol acetyltransferase enzyme (Shalit *et al.* 2003). Acetyl CoA is a central plant metabolite involved in a number of fundamental plant processes, including anabolic and catabolic metabolism as well as signalling and regulatory mechanisms. It is a product of photosynthesis and carbohydrate, amino and fatty acid catabolism while serving as a substrate in mitochondrial respiration. It is also a key substrate used in the biosynthesis of a very large array of both primary and secondary organic compounds. In addition to many non-volatile organic compounds (fatty acids, some amino acids, flavonoids, phenolics, alkaloids, stilbinoids, etc.) (Oliver, Nikolau & Wurtele 2009), acetyl CoA and its precursors pyruvate and phosphoenolpyruvate, provide substrate for a large array of VOCs, including volatile isoprenoids (isoprene, monoterpenes, sesquiterpenes), oxygenated VOCs (acetaldehyde, ethanol, acetic acid, acetone) and fatty acid oxidation products (C₆ green leaf volatiles) (Fig. 1).

Acetylation is a widespread mechanism employed in a large array of processes including the regulation of energy balance, metabolism, and gene expression via protein acetylation (Xing & Poirier 2012), regulating the structural and chemical properties of cell walls through O-acetylation (Pauly & Scheller 2000), and controlling the volatility, solubility, reactivity and biological activity of low molecular

Correspondence: K. Jardine. e-mail: kjardine@lbl.gov

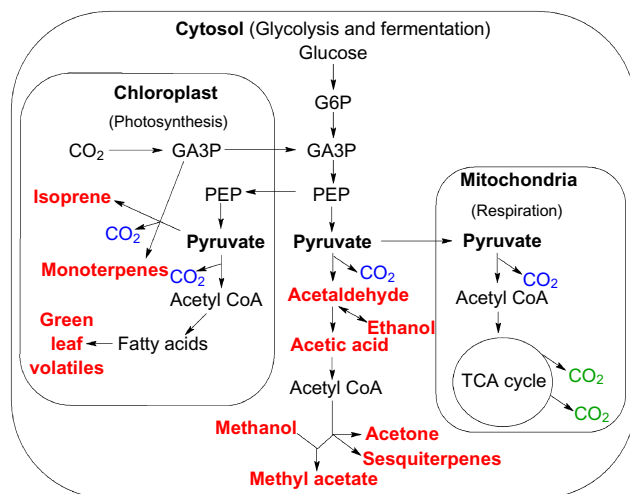


Figure 1. Simplified schematic diagram of CO₂ and VOC metabolism in photosynthetic cells including one putative mechanism for MA biosynthesis from the acetylation of methanol with acetyl CoA. Shown in red are the volatile products of the pyruvate dehydrogenase bypass, mevalonic acid, 2-C-methyl-D-erythritol 4-phosphate (MEP) and fatty acid pathways. CO₂ shown in blue represents carbon originating from the C₁ of pyruvate whereas CO₂ shown in green represents carbon originating from C₂₋₃ of pyruvate. CoA, coenzyme A; MA, methyl acetate; VOC, volatile organic compound.

weight metabolites (Oliver *et al.* 2009, Xing & Poirier 2012). Recently, we demonstrated that photoassimilation of ¹³CO₂ by mesquite branches (*Prosopis velutina*) resulted in strong and rapid ¹³C-labelling of oxygenated VOCs (acetaldehyde, ethanol and acetic acid) and the acetyl group of (Z)-3-hexen-1-yl acetate following light-dark transitions (Jardine *et al.* 2012). These observations support the presence of a pyruvate dehydrogenase bypass pathway (PDH bypass) in plants (Wei *et al.* 2009), which may contribute to acetyl-CoA pools used in a variety of biosynthetic processes and the acetylation of metabolites. Supporting this view, we have utilized pyruvate positional ¹³C-labelling as an innovative tool to trace plant metabolic pathways associated with acetyl CoA metabolism in individual leaves. We showed that like acetyl CoA, the biosynthesis of volatile isoprenoids (isoprene, monoterpenes and sesquiterpenes) and oxygenated VOCs (acetaldehyde, ethanol, acetic acid and acetone) is associated with pyruvate C₁ decarboxylation reactions (Jardine *et al.* 2010c). Pyruvate-2-¹³C feeding of mango leaves (*Mangifera indica*) resulted in a significant incorporation of the ¹³C-label into volatile isoprenoids and oxygenated VOCs. However, when pyruvate-1-¹³C was used, less ¹³C-label was observed in the VOCs produced. In contrast, during a separate study focusing on CO₂ emissions of the Mediterranean shrub *Halimium halimifolium* (Priault, Wegener & Werner 2009; Wegener, Beyschlag & Werner 2010), when pyruvate-1-¹³C was supplied, δ¹³CO₂ continuously increased during the light period. However, when pyruvate-2-¹³C was supplied, the evolved CO₂ was more depleted in ¹³C.

Here we combined techniques for isotopic analysis of VOCs [proton transfer reaction-mass spectrometry (PTR-MS) and

gas chromatography-mass spectrometry (GC-MS)], CO₂ [cavity ringdown spectroscopy (CRDS)] and positional labelling which enables real-time tracing of the fate of the C₁₋₃ atoms of pyruvate into biosynthetic processes or decarboxylation to CO₂. We detected diurnal emissions of methyl acetate (MA), the simplest acetylated metabolite, from vegetative tissue as a tracer of acetyl CoA metabolism in leaf tissues. Currently, sources of MA in the atmosphere are mainly considered anthropogenic and include fossil fuel burning via atmospheric oxidation of ethers and other industrial processes. However, MA is generally considered a common fermentation product in fruits and flowers (Matich *et al.* 2003), but emissions to the atmosphere are rarely reported from leaf tissues. Previously, MA emissions were observed from creosotebush (*Larrea tridentata*) in the Sonoran Desert (Jardine *et al.* 2010a) and mechanically wounded leaves of legumes (Davison *et al.* 2008), suggesting potentially important biogenic sources to the atmosphere. In this study, we present a novel technique termed dynamic pulse chasing with pyruvate positional ¹³C-labelling, which reveals, in real time, the differential fate of C₁ versus C₂₋₃ atoms of pyruvate to MA versus CO₂ production from intact leaves and branches. Further, we investigate the extent to which the biosphere might represent a significant source of MA to the atmosphere. We evaluate the dependence of MA emissions from tropical plants on light and air temperature within a large diverse tropical rainforest mesocosm, and quantify vertical atmospheric MA concentration gradients within and above a primary tropical rainforest in the central Amazon during the 2010 dry and 2011 wet seasons.

MATERIALS AND METHODS

In this study, we utilized 20 potted *H. halimifolium* L. plants grown under controlled light, temperature, and humidity conditions in a walk-in growth chamber at the University of Bielefeld, Germany. Attached or detached branches of *H. halimifolium* were enclosed in one of two glass branch chambers (500 mL volume) and flushed continuously (800 mL min⁻¹) with hydrocarbon-free air, generated by passing room air through a series of three high-purity hydrocarbon traps (Restek Inc., Bellefonte, PA, USA). A third empty glass chamber was used simultaneously as a control. VOC identities, enclosure concentrations and isotopic composition were determined using an online PTR-MS (Ionicon Analytik, Innsbruck, Austria) and a GC-MS (5975C series, Agilent Technologies, Bellefonte, PA, USA) with sample collection/injection using thermal desorption (Unity 2, Markes International, Llantrisant, UK) as described below. In addition, enclosure concentrations of CO₂ and H₂O as well as the stable carbon isotopic composition of CO₂ were determined using a cavity ringdown spectrometer (CRDS, G2101-i, Picarro Inc., Santa Clara, CA, USA). CO₂ and H₂O concentrations entering the enclosures were those of the ambient air and a large (~300 L) buffer volume was utilized to dampen out high frequency variations. Gas samples from control and plant enclosures were connected to a Teflon solenoid valve system (PTFE, Cole-Parmer, Vernon Hills, IL,

USA) via 1/8" O.D. Teflon (PFA) tubing which selected one of up to three enclosure samples (including one empty enclosure) to be continuously analyzed by PTR-MS ($\sim 50 \text{ mL min}^{-1}$) and CRDS ($\sim 50 \text{ mL min}^{-1}$). Each enclosure was measured for 30 min (two enclosures) or 20 min (three enclosures) each hour. In addition, VOC samples from control and plant enclosures were manually collected on thermal desorption tubes and analysed using a GC-MS (see GC-MS section below). All flow rates were controlled with mass flow controllers (Cole-Parmer). Constant light was supplied to the plants over a 12 h period (0800–2000 h) with photosynthetically active radiation (PAR) intensities at the height of the top branch of between 350 and 500 $\mu\text{mol m}^{-2} \text{ s}^{-1}$, depending on the height of the branch. Ambient air temperature (23 °C) and relative humidity (60%) were held constant in the growth chamber while enclosure air temperatures increased during the day up to 28–33 °C. Following trace gas measurements, the branches were harvested and total enclosed leaf area and dry weight were determined.

¹³C-labelling experiments

We followed online VOC and CO₂ emissions and their stable carbon isotope composition using our new dynamic pulse chasing technique, based on positional-specific ¹³C-pyruvate branch feeding. Fresh 20 mM solutions of pyruvate, pyruvate-1-¹³C, pyruvate-2-¹³C and pyruvate-2,3-¹³C were prepared 1 day prior to each pulse chase experiment by dissolving the appropriate amount of each component in 10 mL of tap water. Following the introduction of an attached branch in the enclosure, the stem was cut, placed in tap water and immediately re-cut under water. Thereafter, the stem was quickly transferred into one of the pyruvate solutions in a 1.0 mL Eppendorf tube for 20–180 min. As the solution was taken up by the branch's transpiration stream, fresh pyruvate solution was added to the Eppendorf tube to ensure the branch was continuously immersed. Following this period, the stem was quickly transferred into a second pyruvate solution in a different Eppendorf tube. The solutions were changed in this manner up to 14 times for a single branch. For the first branch in the light, pyruvate solutions were fed during a pulse chase experiment in the following sequence: unlabelled pyruvate, pyruvate-2-¹³C, pyruvate-1-¹³C, pyruvate-2,3-¹³C, unlabelled pyruvate, pyruvate-2-¹³C and pyruvate-1-¹³C. For the second branch, pulse chasing of pyruvate-1-¹³C with pyruvate-2,3-¹³C in the light was repeated seven times, with water (H₂O) delivered at the beginning and end of the experiment as well as after the first pulse chase. Four additional branches were pulse chased with pyruvate-1-¹³C and pyruvate-2,3-¹³C three times in the light, but with darkening of the branch enclosure during the last ~15 min in each solution (Supporting Information Figs S1 & S2). Throughout the pulse-chase experiments, continuous online measurements of the isotopic composition of VOCs (PTR-MS) and CO₂ (CRDS) were made. In a separate set of experiments, three thermal desorption (TD) tube samples were collected in the light and analysed by GC-MS from each of four treatments: (1) a detached branch during continuous pyruvate-1-¹³C feeding; (2) a detached branch

during continuous pyruvate-2-¹³C feeding; (3) an attached branch as a control; and (4) an empty enclosure to determine the system background.

Thermal desorption GC-MS

Enclosure air samples were collected by drawing 200 mL min⁻¹ of enclosure air through a TD tube for 30 min (6.0 L) by connecting a mass flow controller and a pump downstream of the tube. TD tubes were purchased commercially, filled with Tenax TA, graphitized carbon and Carboxen 1000 adsorbents (Markes International). The tube samples were analysed utilizing a Unity 2 thermal desorption system (Markes International) interfaced with a 5975C series gas chromatograph/electron impact mass spectrometer with a triple-axis detector (Agilent Technologies). After loading a tube in the Unity 2 thermal desorption system, the collected samples were dried for 3 min with 30 mL min⁻¹ of ultra-high purity helium (all flow vented out of the split vent) before being transferred to the Unity 2 cold trap (water management cold trap) held at 30 °C by heating to 300 °C for 5 min with 50 mL min⁻¹ of helium. During injection, the trap was heated to 300 °C for 3 min while back-flushing with carrier gas at a flow of 6.5 mL min⁻¹; 5 mL min⁻¹ vented through the split and 1.5 mL min⁻¹ directed to the column (Agilent DB624 60 m × 0.32 mm × 1.8 μm), temperature programmed with an initial hold of 3 min at 40 °C followed by an increase to 220 °C at 6 °C min⁻¹ followed by a hold at 220 °C for 1 min. The mass spectrometer was configured for trace analysis with a 15 times detector gain factor and operated in scan mode (*m/z* 40–300). Identification of MA in TD tube samples was confirmed by comparison of mass spectra with the NIST mass spectral library and with a MA permeation tube standard (Kin-Tek Labs, La Marque, TX, USA) and by comparison of retention times. Identification of other volatiles such as monoterpenes (MTs) and sesquiterpenes (SQTs) was based solely on mass spectra comparison with the NIST mass spectral library

PTR-MS

The target volatiles in ambient air and enclosure samples were analysed using a commercial high sensitivity PTR-MS (Ionicon Analytik, Innsbruck, Austria) that was operated in standard conditions with a drift tube voltage of 600 V, temperature of 40 °C and pressure of 2.0 mb. The following mass to charge ratios (*m/z*) were monitored during each PTR-MS measurement cycle: 21 (H₃¹⁸O⁺), 32 (O₂⁺), 37 (H₂O-H₃O⁺) with a dwell time of 20 ms each. The following *m/z* values were also sequentially measured with a 2 s dwell time and correspond to the protonated molecular weights (parent ions) of the following compounds: *m/z* 33 (methanol), *m/z* 43 (acetyl fragment), *m/z* 45 (acetaldehyde), *m/z* 47 (formic acid + ethanol), *m/z* 59 (acetone), *m/z* 61 (acetic acid), *m/z* 69 (isoprene), *m/z* 75 (methyl acetate), *m/z* 137 (monoterpenes) and *m/z* 205 (sesquiterpenes). During pyruvate ¹³C-labelling studies, PTR-MS signals with a 2 s dwell time were monitored including *m/z* 75 (methyl acetate-1,2-¹²C), *m/z* 76 (methyl

acetate- ^{13}C), m/z 77, (methyl acetate-1,2- ^{13}C), m/z 43, (acetyl fragment- ^{12}C), m/z 44 (acetyl fragment- ^{13}C), m/z 45 (acetyl fragment-1,2- ^{13}C + acetaldehyde). Under the oxidizing conditions of the Amazon atmosphere, m/z 75 is assumed to be the combination of MA and hydroxyacetone (HA), a second-generation oxidation product of isoprene (Karl *et al.* 2007; Yokelson *et al.* 2009; Warneke *et al.* 2011). To quantify MA in branch and mesocosm air samples, the PTR-MS was calibrated to MA using the dynamic solution injection technique as previously described (Jardine *et al.* 2010b). Given that we used the calibration factor based only on MA to estimate the combined atmospheric concentrations of MA + HA within the Amazon canopy, these measurements should be considered rough estimates.

CRDS

The CO_2 concentration and isotopic composition of the sample gas was measured with a CRDS (G2101-i, Picarro Inc.), which enables real-time analysis of the isotopologues $^{13}\text{CO}_2$ and $^{12}\text{CO}_2$ as well as the $\delta^{13}\text{CO}_2$ ratio (‰) of the sample gas relative to the factory-calibrated reference standard Vienna Pee Dee Belemnite (VPDB). Isotope ratios are presented in δ -notation as:

$$\delta^{13}\text{C} = \left(\frac{R_{\text{sample}}}{R_{\text{standard}}} - 1 \right) \times 1000\text{‰} \quad (1)$$

where R_{sample} is the measured $^{13}\text{C}/^{12}\text{C}$ isotope ratio of the sample and R_{standard} is the $^{13}\text{C}/^{12}\text{C}$ isotope ratio of the standard (VPDB). One-minute averages were calculated from the $\delta^{13}\text{C}$ values provided by the CRDS. The CRDS was regularly calibrated with a laboratory reference gas and cross-calibrated to an isotope ratio mass spectrometer (IRMS, Isoprime; Elementar, Hanau, Germany) interfaced to a gas autosampler (Microgas, GV, Manchester, UK) in Bielefeld, Germany.

Amazon field study

Ambient measurements of MA + HA at six heights within and above a primary rainforest canopy were carried out at the TT34 tower (02°35.657' S, 060°12.557' W) in the Reserva Biologica do Cueiras in central Amazonia, 60 km NNW of the city of Manaus, Brazil. The site is run by INPA (Instituto Nacional de Pesquisas da Amazonia) under the Large Scale Biosphere-Atmosphere Experiment in Amazonia (LBA) programme (Martin *et al.* 2010). The vegetation in this area is considered to be undisturbed, mature, *terra firme* rainforest, with a leaf area index of 5–6 and an average canopy height of 30 m (Jardine *et al.* 2011). PTR-MS measurements of ambient MA + HA occurred during the 2010 dry season (2 September–9 November 2010) and 2011 wet season (6 December 2010–27 January 2011). The gradient measurement scheme employed ambient air inlets at six different tower heights (2, 11, 17, 24, 30 and 40 m) sequentially analysed for MA + HA at m/z 75 with a 5 s dwell time (10 min at each inlet, one complete canopy profile per hour). Ambient air (–0.1 m from the tower) was drawn through 1/4 in O.D. heated Teflon tubing using an oil-free diaphragm pump with a sample point to detector delay time of <15 s.

Biosphere 2 mesocosm study

Atmospheric measurements of MA within the Biosphere 2 tropical rainforest (44 × 44 m with a total volume of 26 700 m³) were obtained by drawing air through heated Teflon tubing to a nearby (~25 m) laboratory. The rainforest mesocosm currently comprises 91 species of tropical plants from 41 families, including 73 trees under a flat-topped pyramidal glass enclosure operated as a semi-closed system (Allen, Nelson & Alling 2003). The sampling port was located ~20 m off the ground within 3–5 m of a tower equipped with PAR (SQ120 Quantum sensors, Apogee Instruments, Logan, UT, USA) and vented and shielded temperature and humidity sensors (HMP45c, Vaisala Instruments, Tucson, AZ, USA). Within the laboratory, the PTR-MS analysed the Biosphere 2 tropical rainforest air continuously for MA concentrations between 22 January and 10 March 2010. Every hour, the MA background was determined from hydrocarbon-free air measurements.

RESULTS

Controlled laboratory studies

Attached branches of *H. halimifolium*, a mediterranean shrub of the Cistaceae family previously suspected to be a high VOC emitter (Priault *et al.* 2009), were found to be a significant emitters of MTs and SQTs (Fig. 2). For the three attached branches studied, mean midday emission rates (1200–1300 h) were $0.10 \pm 0.06 \text{ nmol m}^{-2} \text{ s}^{-1}$ for total MTs and $0.26 \pm 0.21 \text{ nmol m}^{-2} \text{ s}^{-1}$ for total SQTs (mean \pm one standard deviation for three branches). In addition, emissions of the oxygenated VOCs acetaldehyde, methanol, ethanol, acetic acid, acetone, and MA were observed (Fig. 2 and Supporting Information Fig. S3). Surprisingly, mean midday emission rates of MA were high ($0.39 \pm 0.22 \text{ nmol m}^{-2} \text{ s}^{-1}$) and thus in a comparable range to those of MTs and SQTs. However, while daytime emissions for MTs and SQTs were much higher than at night, significant night-time emissions were observed for MA, particularly early in the morning before the light turned on. Continuous volatile emission rate measurements at high-time resolution revealed enhanced MA and methanol diurnal dynamics. In the dark at night, a slow increase in MA and methanol emissions occurred, followed by a large morning burst within 5 min of switching on the light source (Fig. 2b).

As MA emissions from vegetative tissues are rarely reported, we used GC-MS to verify its presence in the volatile emission blend from attached *H. halimifolium* branches (Fig. 3a). A strong peak was observed in the GC-MS chromatogram at 8.12 min in the enclosure samples with a branch while the empty enclosure samples did not produce a detectable peak. The identification of the GC-MS peak at 8.12 min was verified as MA by a strong match (>95% confidence) with the NIST 2008 mass spectral library and by the identical retention time and mass spectra of an MA gas phase permeation tube standard (Fig. 3a). Under the conditions studied, MA produced the acetyl fragment (CH_3CO , m/z 43) in both the PTR-MS and GC-MS. While MA under proton

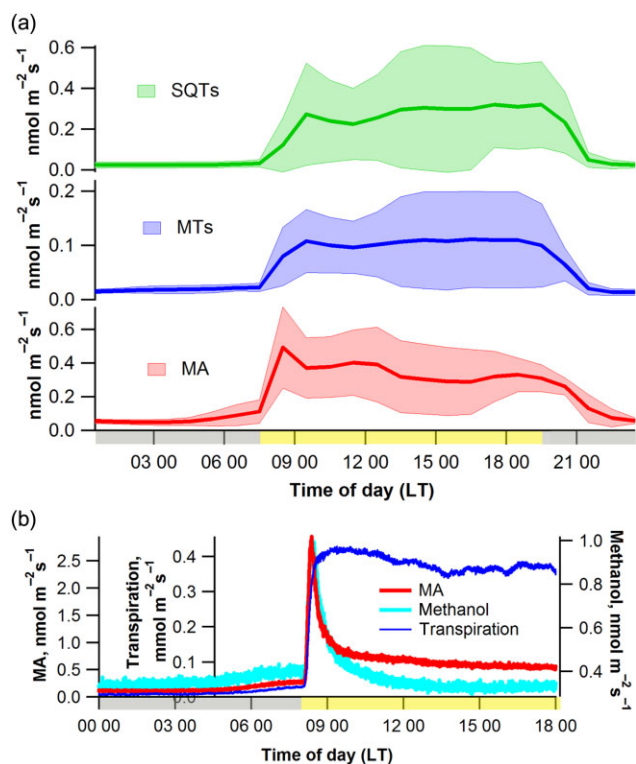


Figure 2. Representative time series plot showing diurnal dynamics of VOC emissions from attached *H. halimifolium* branches with shaded areas indicating dark (grey) and light (yellow) periods. (a) Mean diurnal emission rates of MA, total MTs, and total SQTs from three attached *H. halimifolium* branches. Shaded regions represent mean emission rates \pm one standard deviation. (b) High temporal resolution measurements of MA and methanol emission rates together with transpiration rates showing a large emission burst shortly after switching on the light source. MA, methyl acetate; MT, monoterpenes; SQT, sesquiterpenes; VOC, volatile organic compound.

transfer ionization in the PTR-MS produced a strong signal at m/z 75 corresponding to the protonated parent ion, electron ionization in the GC-MS produced the parent ion at m/z 74. Using the dynamic solution injection technique for calibration (Jardine *et al.* 2010b), the PTR-MS response to MA at m/z 75 was found to be highly sensitive (175 cps/ppbv) and linear ($R^2 = 0.999$) across gas-phase concentrations in the range of 0–28.2 ppbv. These observations are consistent with a previous study on PTR-MS fragmentation patterns of MA which found the majority of signal at the protonated parent ion (m/z 75) with 9% occurring as the acetyl fragment (m/z 43) (Buhr, van Ruth & Delahunty 2002).

In order to further explore the metabolic origin of MA emissions from *H. halimifolium* branches, we performed positional-specific ^{13}C -pyruvate branch feeding experiments to evaluate the hypothesis that pyruvate is used as a substrate in the biosynthesis of MA. The results of GC-MS analysis of air samples collected from detached branches placed in the pyruvate-1- ^{13}C solution versus the pyruvate-2- ^{13}C solution is shown in Fig. 3b. Upon electron impact ionization, the mass spectrum of MA is dominated by the acetyl fragment (m/z

43) and the parent ion (m/z 74). Ions at m/z 44 and m/z 75 represent the singly ^{13}C -labelled versions of the acetyl fragment and parent ions, respectively. Relative GC-MS mass spectra of MA peaks from attached *H. halimifolium* branches and detached *H. halimifolium* branches under pyruvate-1- ^{13}C solution displayed similar relative mass spectra, with relative ion ratios consistent with natural ^{13}C -abundance samples. For example, expected relative ion intensities m/z 43/(43 + 44) for the acetyl fragment for natural abundance samples is 2.2% and measured values were $3.6 \pm 0.4\%$ and $4.6 \pm 0.1\%$ for samples collected from attached branches and branches fed with pyruvate-1- ^{13}C , respectively. Likewise, expected relative ion intensities m/z 74/(74 + 75) for the MA parent ion is 3.3% and measured values were $3.9 \pm 0.6\%$ and $6.0 \pm 0.2\%$ for samples collected

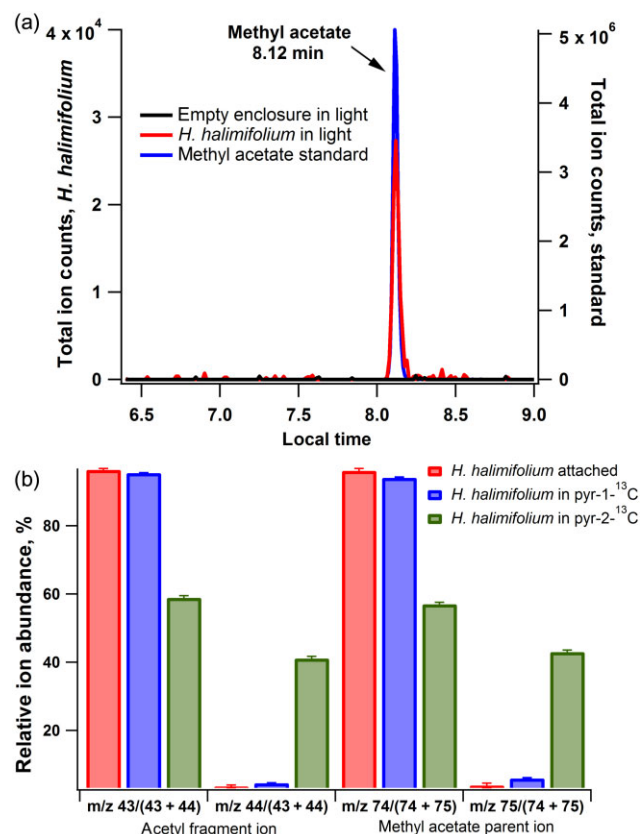


Figure 3. GC-MS analysis of MA emissions from *H. halimifolium* under natural conditions and during positional-specific ^{13}C -labelled pyruvate branch feeding. (a) Example GC-MS total ion count chromatograms showing the presence of MA from a permeation tube standard containing MA and the volatile emissions of an attached *H. halimifolium* branch. (b) GC-MS relative ion abundances of methyl acetate peaks (mean \pm 1 standard deviation, $n = 3$) over the ranges m/z 43–44 (^{12}C and ^{13}C -acetyl fragment ions) and m/z 74–75 (^{12}C and ^{13}C -methyl acetate ions) in air samples including: (1) emissions from an attached *H. halimifolium* branch; (2) emissions from a detached *H. halimifolium* branch in 20 mM pyruvate-1- ^{13}C ; and (3) emissions from a detached *H. halimifolium* branch in 20 mM pyruvate-2- ^{13}C (red, blue and green bars respectively). GC-MS, gas chromatography-mass spectrometry; MA, methyl acetate.

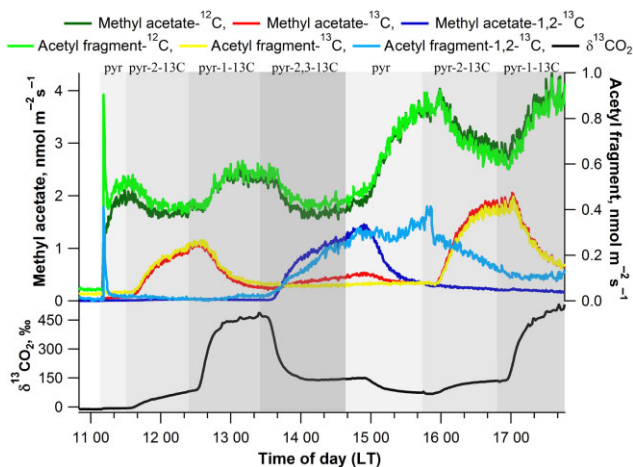


Figure 4. Representative emission of MA and acetyl fragment isotopologues with 0–2 ^{13}C atoms together with $\delta^{13}\text{CO}_2$ during a dynamic pulse chase experiment with a single-detached *H. halimifolium* branch showing real-time ^{13}C -labelling dynamics at low frequency. MA, methyl acetate.

from attached branches and branches fed with pyruvate-1- ^{13}C , respectively. Thus, no notable effect occurred from detaching the branches, nor was a large labelling of MA recorded after feeding pyruvate-1- ^{13}C . However, the slight enhancement in ^{13}C -MA under pyruvate-1- ^{13}C may be due to the refixation of the C_1 carbon atom of pyruvate during photosynthesis, followed by incorporation into MA as was previously observed for isoprene and monoterpenes (Jardine *et al.* 2010c). In contrast, a strong ^{13}C -enrichment in both the acetyl fragment ion and the MA parent ion was observed in samples collected from branches fed with pyruvate-2- ^{13}C . Relative ion intensities for the acetyl fragment ion and the MA parent ion from these samples was $41.1 \pm 0.6\%$ and $43.0 \pm 0.5\%$, respectively.

In order to investigate the real-time dynamics of MA biosynthesis and to further elucidate the different fates of the C_1 , C_2 and C_3 carbon atoms of pyruvate, we developed a technique termed ‘Dynamic ^{13}C -pulse chase’ which couples rapid changes in positional-specific ^{13}C -pyruvate plant feeding solutions with real-time MA and $\delta^{13}\text{CO}_2$ detection using PTR-MS and CRDS. In the first experiment, 20 mM solutions of pyruvate, pyruvate-1- ^{13}C , pyruvate-2- ^{13}C and pyruvate-2,3- ^{13}C were fed sequentially through the transpiration stream of a detached *H. halimifolium* branch for 20–70 min each, followed by an additional cycle through 20 mM pyruvate, pyruvate-2- ^{13}C and pyruvate-1- ^{13}C solutions.

Figure 4 shows real-time measurements of MA and its acetyl fragment together with $\delta^{13}\text{CO}_2$ in response to the feeding solutions. We found that the emission dynamics of MA and its acetyl fragment isotopologues with 0–2 ^{13}C atoms can be monitored in real time using PTR-MS. Upon placing the branch in the unlabelled pyruvate solution (at 1110 h local time), emissions of ^{12}C -MA and its ^{12}C -acetyl fragment dominated emissions of all other MA isotopologues (green lines Fig. 4). During this time, $\delta^{13}\text{CO}_2$ ranged slightly above

the background values ($-12\% \pm 1\%$ throughout the experiment) due to photosynthetic discrimination against ^{13}C . Within 10 min after placing the branch in the pyruvate-2- ^{13}C solution (at 1125 h), emissions of MA- ^{12}C and its acetyl- ^{12}C fragment began to decline at the same time that strong emissions of MA- ^{13}C and its acetyl- ^{13}C fragment emerged. Concurrent with the increase in singly ^{13}C -labelled MA was an increase in $\delta^{13}\text{CO}_2$. At 1225 h, the solution was changed to pyruvate-1- ^{13}C and within 10 min, emissions of MA- ^{12}C and its acetyl- ^{12}C fragment began to increase again while emissions of MA- ^{13}C and its acetyl- ^{13}C fragment began to decline. At the same time, $\delta^{13}\text{CO}_2$ values increased strongly. At 1325 h, the solution was switched to pyruvate-2,3- ^{13}C and within 10 min declining emissions of MA- ^{12}C and acetyl- ^{12}C fragment was detected with an increase in MA-1,2- ^{13}C and acetyl-1,2- ^{13}C fragment. At the same time, $\delta^{13}\text{CO}_2$ markedly decreased. At 1445 h, the branch was returned to the unlabelled pyruvate solution and within 10 min emissions of MA- ^{12}C and its acetyl- ^{12}C fragment began to increase while emissions of MA-1,2- ^{13}C and its acetyl-1,2- ^{13}C fragment began to decline. However, the PTR-MS signal for the acetyl-1,2- ^{13}C fragment (m/z 45) began to increase again and is likely due to an interference by acetaldehyde (also appearing at m/z 45). At 1545 and 1650 h, the branch was placed back in the pyruvate-2- ^{13}C solution and the pyruvate-1- ^{13}C solution, respectively, with similar MA, acetyl fragment and CO_2 ^{13}C -labelling patterns as the first pulse chase in these solutions.

A separate detached *H. halimifolium* branch was used to demonstrate the possibility of rapidly changing the positional specific ^{13}C -pyruvate solutions in order to produce a continuous non-steady state time series highlighting the fast response in ^{13}C -labelled MA and CO_2 emissions, and to repeatedly demonstrate the different fates of the pyruvate C_1 atom versus the $\text{C}_{2,3}$ atoms into MA and CO_2 emissions by chasing pyruvate-2,3- ^{13}C with pyruvate-1- ^{13}C multiple times on the same branch (Fig. 5). In this experiment, the branch was first placed in tap water before chasing pyruvate-2,3- ^{13}C with pyruvate-1- ^{13}C (in each solution for approximately 20 min), followed by incubation in tap water. Thereafter, pyruvate-2,3- ^{13}C was again chased with pyruvate-1- ^{13}C six additional times before finishing back in tap water. The results show the same pattern as described in the experiment shown in Fig. 4. Under pyruvate-2,3- ^{13}C feeding, emissions of the doubly labelled MA-2,3- ^{13}C and acetyl-2,3- ^{13}C fragment are induced at the expense of MA- ^{12}C and acetyl- ^{12}C fragment emissions. In contrast, under pyruvate-1- ^{13}C feeding, emissions of the MA- ^{12}C and acetyl- ^{12}C fragment increase again at the expense of the doubly labelled MA-1,2- ^{13}C and acetyl-1,2- ^{13}C fragment. While pyruvate-2,3- ^{13}C feeding lead to a ^{13}C -enrichment in CO_2 emissions relative to tap water feeding, pyruvate-1- ^{13}C feeding resulted in a much higher ^{13}C -enrichment in CO_2 emissions. Throughout the pulse-chase experiment, CO_2 concentrations within the enclosure remained relatively constant with a range of 307–331 ppmv with an incoming CO_2 concentration in the range of 400–410 ppmv. This indicates that 20 mM pyruvate feeding does not significantly inhibit photosynthesis or alter net CO_2 assimilation.

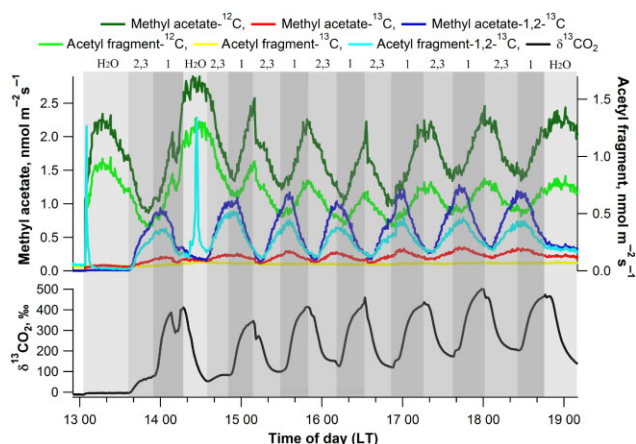


Figure 5. Representative emission of isotopologues of protonated methyl acetate and acetyl fragments with 0–2 ^{13}C atoms together with $\delta^{13}\text{CO}_2$ during a dynamic pulse chase experiment with a single-detached *H. halimifolium* branch showing real-time ^{13}C -labelling dynamics at high frequency. Pulse chasing of 20 mM pyruvate-1- ^{13}C (1) with pyruvate-2,3- ^{13}C (2,3) was repeated seven times with water (H_2O) delivered at the beginning and end of the experiment as well as after the first pulse chase.

Tropical rainforest mesocosm and field studies

Mean ambient air concentrations of MA together with air temperature and PAR at 20 m height within the Biosphere 2 mesocosm is shown in Fig. 6 (917 h during 22 January–10 March 2010). Whole mesocosm ambient air concentrations of MA displayed a strong diurnal cycle with maxima occurring in early afternoon (~1400 h) with values up to 0.6 ppbv. Maximum air temperature also peaked in early afternoon (~14:00 h) whereas PAR peaked earlier at midday (~1230 h). Significant ambient concentrations of MA up to 0.2 ppbv occurred at night, supporting the possibility of night-time emissions as observed in the laboratory study (Fig. 2). It is apparent that ambient MA concentrations inside the rainforest mesocosm reported here and those of the oxygenated VOCs (acetaldehyde, ethanol, acetic acid and acetone), and volatile isoprenoids (isoprene, monoterpenes and sesquiterpenes) previously reported (Pegoraro *et al.* 2005; Jardine *et al.* 2010c) all share a similar diurnal pattern. These observations are consistent with the positional-specific ^{13}C -pyruvate labelling experiments that demonstrate pyruvate as a common precursor. While these results suggest that tropical ecosystems can emit MA into the atmosphere, field studies are needed to further explore this possibility.

In order to investigate the potential role of a primary tropical rainforest in the central Amazon in the biosphere–atmosphere exchange of MA + HA during the 2010 dry and 2011 wet seasons, we collected continuous *in situ* vertical concentration profiles within and above the ~30 m canopy, utilizing a high-sensitivity PTR-MS (Fig. 7a–d). Similar to the tropical mesocosm studies, ambient air concentrations at all heights followed strong diurnal patterns with maxima in the early afternoon (1200–1300 h). MA + HA concentrations in the dry season were generally higher than those in the wet

season with maximum mean values similar to those in the Biosphere 2 rainforest mesocosm (dry: 0.3 ppbv, wet: 0.1 ppbv, Biosphere 2: 0.4 ppbv). During the 2010 dry season, the mean vertical gradient of ambient MA + HA in the early afternoon (1300–1400 h) indicated net ecosystem deposition at the Amazon forest tower site, with the concentrations highest above the canopy and declining with depth through the canopy (Fig. 7b). In contrast, during the 2011 wet season, the highest ambient concentrations were observed within the canopy (17 m) rather than above the canopy (40 m) (Fig. 7d). This implies that the ecosystem was a net emission source during the wet season. In both the wet and the dry seasons, the lowest ambient concentrations observed were near the ground (2 m). This may be due to low MA production rates by soils and understorey vegetation under reduced light and temperature conditions, together with dry/wet deposition and active consumption of MA.

DISCUSSION

Although MA is generally considered a common fermentation product in plants as it is often found in fruits (de Avila *et al.* 2012), vegetables (Forney, Mattheis & Austin 1991) and flowers (Matich *et al.* 2003), MA emissions are rarely reported from leaf tissues. Currently, sources of MA in the atmosphere are mainly considered anthropogenic and include fossil fuel burning via atmospheric oxidation of ethers used in automotive fuel additives (Christensen, Ball &

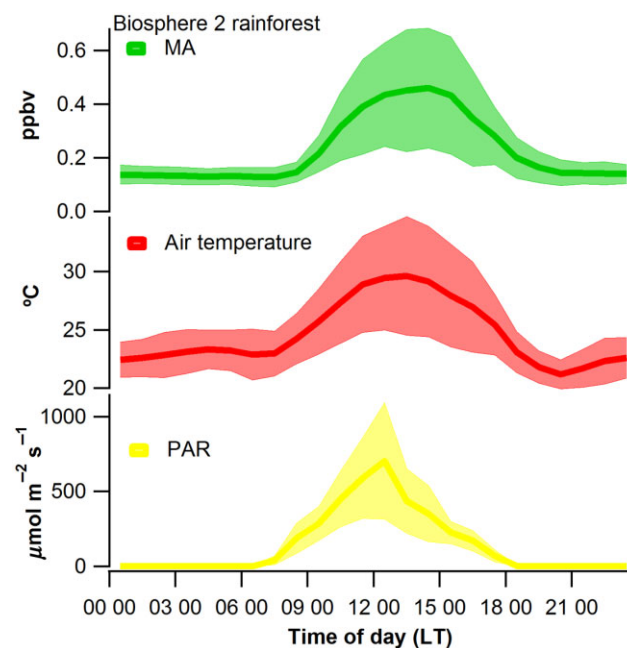


Figure 6. Mean diurnal profiles of MA atmospheric concentrations at 20 m height in a large enclosed tropical rainforest mesocosm at Biosphere 2, Arizona during spring 2010 (917 h during 22 January–10 March 2010). Also shown are mean diurnal pattern of air temperature and PAR at 20 m height. The shaded regions represent mean value \pm one standard deviation. MA, methyl acetate; PAR, photosynthetically active radiation.

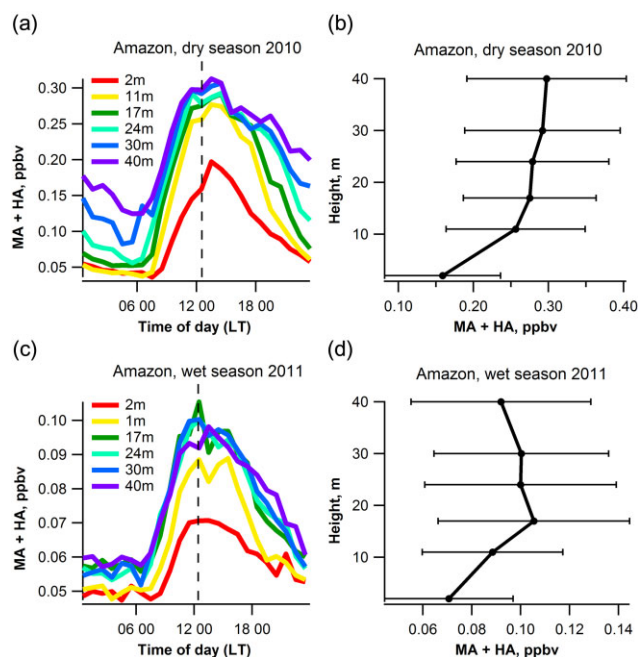


Figure 7. Mean diurnal atmospheric profiles of PTR-MS signals attributed to MA + HA within and above a ~30 m tall primary rainforest in the central Amazon during the (a) 2010 dry season (538 h during 2 September–9 November 2010) and (c) 2011 wet season (513 h during 6 December 2010–27 January 2011) season. Also shown are mean midday (1200–1300 h) vertical concentration gradients during the dry (b) and wet (d) seasons, with error bars representing \pm one standard deviation. HA, hydroxyacetone; MA, methyl acetate; PTR-MS, proton transfer reaction-mass spectrometry.

Wallington 2000), biomass burning (Yokelson *et al.* 2009), the evaporation as a solvent in the chemical industry (e.g. the carbonylation of methanol during the production of acetic acid) (Filella, Peñuelas & Llusà 2006), and during the manufacturing and use of perfumes and food flavourings (Zoeller *et al.* 1992). In this study, we show that PTR-MS is a highly sensitive technique for the study of gas-phase MA and provide the first clear evidence based on a combined PTR-MS and GC-MS approach that leaf tissues can emit MA in the daytime at significant rates, exceeding $0.5 \text{ nmol m}^{-2} \text{ s}^{-1}$. We found that coincident with a large increase in transpiration rates, both methanol and MA emissions dramatically increase in the morning when the light was switched on (Fig. 2b). This suggests that similar to what has been demonstrated for methanol (Nemecek-Marshall *et al.* 1995), MA emissions are under tight stomatal regulation and can accumulate within internal plant aqueous phases at night, followed by emission bursts upon stomatal opening in the morning (Niinemets & Reichstein 2003).

To gain additional insight into the biosynthesis of MA, we developed a new technique to study carbon allocation in plants termed dynamic pulse chasing which combines positional ^{13}C -labelled pyruvate feeding via the transpiration stream with real-time isotopic analysis of MA and CO_2 emissions. The power of the technique stems from its ability

to follow the differential allocation of C_1 versus C_2 and C_3 carbon atoms of pyruvate into biosynthetic and carbon decarboxylation metabolism in plants in real time and may potentially be applied at a number of spatial scales from individual leaves to whole trees. Using this technique at the branch scale, we found that the C_1 atom of pyruvate is decarboxylated during MA biosynthesis while the C_2 and C_3 atoms are directly incorporated into MA. Unlabelled pyruvate and pyruvate- $1\text{-}^{13}\text{C}$ branch feeding did not result in strong ^{13}C -labelling of MA and its acetyl fragment. In contrast, feeding with pyruvate- $2\text{-}^{13}\text{C}$ and pyruvate- $2,3\text{-}^{13}\text{C}$ resulted in the biosynthesis and emission of singly and doubly ^{13}C -labelled MA and its acetyl fragment, respectively, at the expense of their corresponding ^{12}C isotopologues. Relative to feeding with unlabelled pyruvate, branch feeding with pyruvate- $1\text{-}^{13}\text{C}$ resulted in a strong ^{13}C -enrichment in emitted CO_2 . ^{13}C -enrichment in emitted CO_2 was also observed to be significant during pyruvate- $2\text{-}^{13}\text{C}$ and to a greater extent pyruvate- $2,3\text{-}^{13}\text{C}$ branch feeding, albeit to a lower extent than pyruvate- $1\text{-}^{13}\text{C}$. These results indicate that the $\text{C}_{2,3}$ atoms of pyruvate are incorporated into MA during *de novo* biosynthesis but that a certain proportion gets also decarboxylated in the light. The tricarboxylic acid cycle (TCA) has been found to be markedly inhibited in the light (Tcherkez *et al.* 2005; Werner *et al.* 2009) as it may undergo a major re-organization during illumination (Sweetlove *et al.* 2010). Some CO_2 may have also evolved from the heterotrophic tissue (stems) of the enclosed branches. Nevertheless, decarboxylation from the C_1 atom of pyruvate was much enhanced pointing towards marked decarboxylation during MA biosynthesis and other processes in the light.

While stronger ^{13}C -labelling of MA (Figs 4 & 5, Supporting Information S1 & S2) and MTs (Supporting Information Figs S4 & S5) were observed under pyruvate- $2\text{-}^{13}\text{C}$ and pyruvate- $2,3\text{-}^{13}\text{C}$ than pyruvate- $1\text{-}^{13}\text{C}$, their temporal ^{13}C -labelling responses to changes in ^{13}C -pyruvate solutions showed important differences. Whereas MA and CO_2 responded within minutes (Figs 4 & 5) to changes in ^{13}C -pyruvate solutions, a large delay (20–30 min) was observed for MTs (Figs S4 & S5). If allowed to reach steady state under a given ^{13}C -pyruvate solution, the dynamics following an immediate change to a different ^{13}C -pyruvate solution could be exploited to gain new understanding of biosynthesis and degradation rates and pool sizes. Our observations suggest that pyruvate and acetyl CoA are rapidly turned over in plants and hypothesize that MA may derive from the acetylation of methanol by acetyl CoA catalyzed by an alcohol acetyl-transferase enzyme. In contrast, the kinetics of ^{13}C incorporation into MT emissions is slower, possibly due in part to a larger pool size and higher number of $\text{C}_{2,3}$ pyruvate equivalents needed for MT biosynthesis.

The lower incorporation of the C_1 atom of pyruvate into MA relative to the C_2 atom was also observed for the oxygenated VOCs acetaldehyde, ethanol and acetic acid (Supporting Information Fig. S6). This is consistent with our previous findings from mango leaves where the incorporation of the C_1 atom of pyruvate into VOCs including volatile isoprenoids (isoprene, MTs, SQTs) and oxygenated VOCs

(acetaldehyde, ethanol, acetic acid and acetone) was lower relative to the C₂ atom (Jardine *et al.* 2010c). These observations highlight the fact that the biosynthesis of a large array of both primary and secondary organic compounds is associated with pyruvate C₁ decarboxylations, which represent a non-mitochondrial source of CO₂ that must contribute to net CO₂ fluxes. Still, little is known on the quantitative contribution from different CO₂ sources originating from different metabolic pathways to the overall CO₂ flux (Werner *et al.* 2011). For example, the biosynthesis of many non-volatile organic compounds is well known to derive from acetyl CoA (fatty acids, some amino acids, flavonoids, phenolics, alkaloids, stilbinoids, etc.) (Oliver *et al.* 2009), and therefore must also be associated with pyruvate C₁ decarboxylations. Thus, our study uses MA emissions as a tracer of CO₂ production not directly associated with TCA decarboxylations and its associated ATP and reductant production during oxidative phosphorylation reactions in mitochondria. As mitochondrial respiration is known to be partially inhibited in the light (Atkin, Evans & Siebke 1998) while biosynthetic processes are active, future studies should aim to quantitatively evaluate the role of pyruvate C₁ versus C_{2,3} decarboxylations during photosynthesis.

We also presented preliminary evidence that a whole tropical forest mesocosm and a primary rainforest ecosystem in the central Amazon can emit MA at rates sufficiently high to be detected in the atmosphere using PTR-MS. However, previous atmospheric studies using PTR-MS focusing on m/z 75 have suggested that this signal in complex forest atmospheres arises not only from MA but also from hydroxyacetone (HA), a second-generation oxidation product of isoprene (Karl *et al.* 2007; Yokelson *et al.* 2009; Warneke *et al.* 2011). Our vertical gradient data within and above the central Amazon canopy suggest that during the dry season of 2010, elevated ambient concentrations of HA from isoprene oxidation in the troposphere as well as both MA and HA emissions from biomass burning resulted in net uptake by the ecosystem (highest concentrations above the canopy and decreasing within the canopy during mid-day). However, during the wet season of 2011, m/z 75 signals may have been more strongly influenced by MA emissions from vegetation (highest concentrations within the canopy and decreasing above the canopy during mid-day). However, these findings remain speculative because we did not verify the presence of MA or HA using GC-MS nor determine the interference of additional compounds on ambient m/z 75 PTR-MS signals. Thus, additional biosphere-atmosphere studies using techniques able to selectively quantify MA and other acetate esters in the atmosphere are needed in order to verify terrestrial MA emissions to the atmosphere and their atmospheric and ecological significance.

ACKNOWLEDGMENTS

This research was supported by the Office of Biological and Environmental Research of the U.S. Department of Energy under Contract No. DE-AC02-05CH11231 as part of their Terrestrial Ecosystem Science Program. Additional funding

for this project came from the Phileology Foundation of Fort Worth, Texas, the National Science Foundation (CHE 0216226), and the Germany Science Foundation (DFG, WE 2681/5-1). We greatly thank the helpful edits, comments and discussions from Pawel Misztal, Nick Hewitt and Peter Harley.

CONFLICT OF INTEREST

The authors have a patent submitted for the Dynamic ¹³C-pulse chase technique.

REFERENCES

- Allen J.P., Nelson M. & Alling A. (2003) The legacy of Biosphere 2 for the study of biospherics and closed ecological systems. *Advances in Space Research* **31**, 1629–1639.
- Atkin O.K., Evans J.R. & Siebke K. (1998) Relationship between the inhibition of leaf respiration by light and enhancement of leaf dark respiration following light treatment. *Australian Journal of Plant Physiology* **25**, 437–443.
- de Avila J.M.M., Toralles R.P., Cantillano R.F.F., Peralba M.D.R. & Pizzoloto T.M. (2012) Influence of planting system and cold storage on the physical-chemical characteristics and volatile compounds development in strawberries. *Ciência Rural* **42**, 2265–2271.
- Buhr K., van Ruth S. & Delahunty C. (2002) Analysis of volatile flavour compounds by proton transfer reaction-mass spectrometry: fragmentation patterns and discrimination between isobaric and isomeric compounds. *International Journal of Mass Spectrometry* **221**, 1–7.
- Chehab E.W., Kaspi R., Savchenko T., Rowe H., Negre-Zakharov F., Kliebenstein D. & Dehesh K. (2008) Distinct roles of jasmonates and aldehydes in plant-defense responses. *PLoS ONE* **3**, e1904.
- Chehab W., Kaspi R., Savchenko T. & Dehesh K. (2010) Hexenyl acetate mediates indirect plant defense responses. *Proceedings of ANAS (Biological Sciences)* **65**, 145–151.
- Christensen L.K., Ball J.C. & Wallington T.J. (2000) Atmospheric oxidation mechanism of methyl acetate. *Journal of Physical Chemistry A* **104**, 345–351.
- Davison B., Brunner A., Ammann C., Spirig C., Jocher M. & Neftel A. (2008) Cut-induced VOC emissions from agricultural grasslands. *Plant Biology* **10**, 76–85.
- Dudareva N., Raguso R.A., Wang J.H., Ross E.J. & Pichersky E. (1998) Floral scent production in *Clarkia breweri* – III. Enzymatic synthesis and emission of benzenoid esters. *Plant Physiology* **116**, 599–604.
- Engelberth J., Alborn H.T., Schmelz E.A. & Tumlinson J.H. (2004) Airborne signals prime plants against insect herbivore attack. *Proceedings of the National Academy of Sciences of the United States of America* **101**, 1781–1785.
- Fall R., Karl T., Hansel A., Jordan A. & Lindinger W. (1999) Volatile organic compounds emitted after leaf wounding: on-line analysis by proton-transfer-reaction mass spectrometry. *Journal of Geophysical Research-Atmospheres* **104**, 15963–15974.
- Filella I., Peñuelas J. & Llusà J. (2006) Dynamics of the enhanced emissions of monoterpenes and methyl salicylate, and decreased uptake of formaldehyde, by *Quercus ilex* leaves after application of jasmonic acid. *New Phytologist* **169**, 135–144.
- Forney C.F., Mattheis J.P. & Austin R.K. (1991) Volatile compounds produced by broccoli under anaerobic conditions. *Journal of Agricultural and Food Chemistry* **39**, 2257–2259.
- Guenther A., Hewitt C.N., Erickson D., *et al.* (1995) A global-model of natural volatile organic-compound emissions. *Journal of Geophysical Research-Atmospheres* **100**, 8873–8892.
- Guenther A.B., Jiang X., Heald C.L., Sakulyanontvittaya T., Duhl T., Emmons L. & Wang X. (2012) The Model of Emissions of Gases and Aerosols from Nature version 2.1 (MEGAN2.1): an extended and updated framework for modeling biogenic emissions. *Geoscientific Model Development Discussions* **5**, 1–58.
- Guterman I., Masci T., Chen X.L., Negre F., Pichersky E., Dudareva N., Weiss D. & Vainstein A. (2006) Generation of phenylpropanoid pathway-derived volatiles in transgenic plants: rose alcohol acetyltransferase produces phenylethyl acetate and benzyl acetate in petunia flowers. *Plant Molecular Biology* **60**, 555–563.

- Hansen K., Poll L., Olsen C.E. & Lewis M.J. (1992) The influence of oxygen concentration in storage atmospheres on the post-storage volatile ester production of Jonagold Apples. *LWT-Food Science and Technology* **25**, 457–461.
- Herderich M.J., Siebert T., Parker M., Capone D. & Jeffery D. (2010) Spice up your life: analysis of key aroma compounds in Shiraz. *Abstracts of Papers of the American Chemical Society* **240**, 103-AGFD.
- Jardine K., Abrell L., Kurc S.A., Huxman T., Ortega J. & Guenther A. (2010a) Volatile organic compound emissions from *Larrea tridentata* (creosotebush). *Atmospheric Chemistry and Physics* **10**, 12191–12206.
- Jardine K., Henderson W., Huxman T. & Abrell L. (2010b) Dynamic solution injection: a new method for preparing pptv & ppbv standard atmospheres of volatile organic compounds. *Atmospheric Measurement Techniques* **3**, 1569–1576.
- Jardine K., Sommer E., Saleska S., Huxman T., Harley P. & Abrell L. (2010c) Gas phase measurements of pyruvic acid and its volatile metabolites. *Environmental Science and Technology* **44**, 2454–2460.
- Jardine K., Abrell L., Yanez Serrano A.M., et al. (2011) Ecosystem-scale compensation points of formic and acetic acid in the central Amazon. *Biogeosciences* **8**, 3709–3720.
- Jardine K., Barron-Gafford G.A., Norman J.P., et al. (2012) Green leaf volatiles and oxygenated metabolite emission bursts from mesquite branches following light-dark transitions. *Photosynthesis Research* **113**, 321–333.
- Karl T.G., Christian T.J., Yokelson R.J., Artaxo P., Hao W.M. & Guenther A. (2007) The Tropical Forest and Fire Emissions Experiment: method evaluation of volatile organic compound emissions measured by PTR-MS, FTIR, and GC from tropical biomass burning. *Atmospheric Chemistry and Physics* **7**, 5883–5897.
- Knudsen J.T., Tollsten L., Groth I., Bergstrom G. & Raguso R.A. (2004) Trends in floral scent chemistry in pollination syndromes: floral scent composition in hummingbird-pollinated taxa. *Botanical Journal of the Linnean Society* **146**, 191–199.
- Martin S.T., Andreae M.O., Althausen D., et al. (2010) An overview of the Amazonian Aerosol Characterization Experiment 2008 (AMAZE-08). *Atmospheric Chemistry and Physics* **10**, 11415–11438.
- Matich A.J., Young H., Allen J.M., Wang M.Y., Fielder S., McNeillage M.A. & MacRae E.A. (2003) Actinidia arguta: volatile compounds in fruit and flowers. *Phytochemistry* **63**, 285–301.
- Mondello L., Verzera A., Previti P., Crispo F. & Dugo G. (1998) Multidimensional capillary GC-GC for the analysis of complex samples. 5. Enantiomeric distribution of monoterpene hydrocarbons, monoterpene alcohols, and linalyl acetate of bergamot (*Citrus bergamia* Risso et Poiteau) oils. *Journal of Agricultural and Food Chemistry* **46**, 4275–4282.
- Nemecek-Marshall M., MacDonald R.C., Franzen J.J., Wojciechowski C.L. & Fall R. (1995) Methanol emission from leaves: enzymatic detection of gas-phase methanol and relation of methanol fluxes to stomatal conductance and leaf development. *Plant Physiology* **108**, 1359–1368.
- Niinemets U. & Reichstein M. (2003) Controls on the emission of plant volatiles through stomata: differential sensitivity of emission rates to stomatal closure explained. *Journal of Geophysical Research-Atmospheres* **108**, 4208.
- Oliver D.J., Nikolau B.J. & Wurtele E.S. (2009) Acetyl-CoA-Life at the metabolic nexus. *Plant Science* **176**, 597–601.
- Pauly M. & Scheller H.V. (2000) O-Acetylation of plant cell wall polysaccharides: identification and partial characterization of a rhamnogalacturonan O-acetyl-transferase from potato suspension-cultured cells. *Planta* **210**, 659–667.
- Pegoraro E., Abrell L., Van Haren J., Barron-Gafford G., Grieve K.A., Malhi Y., Murthy R. & Lin G.H. (2005) The effect of elevated atmospheric CO₂ and drought on sources and sinks of isoprene in a temperate and tropical rainforest mesocosm. *Global Change Biology* **11**, 1234–1246.
- Pellegrini E., Cioni P.L., Francini A., Lorenzini G., Nali C. & Flamini G. (2012) Volatiles emission patterns in poplar clones varying in response to ozone. *Journal of Chemical Ecology* **38**, 924–932.
- Priault P., Wegener F. & Werner C. (2009) Pronounced differences in diurnal variation of carbon isotope composition of leaf respired CO₂ among functional groups. *New Phytologist* **181**, 400–412.
- Ramey D.D. & Ough C.S. (1980) Volatile ester hydrolysis or formation during storage of model solutions and wines. *Journal of Agricultural and Food Chemistry* **28**, 928–934.
- Rasmussen R. (1972) What do hydrocarbons from trees contribute to air-pollution. *Journal of the Air Pollution Control Association* **22**, 537–543.
- Shalit M., Guterman I., Volpin H., et al. (2003) Volatile ester formation in roses. Identification of an acetyl-coenzyme A. Geraniol/citronellol acetyltransferase in developing rose petals. *Plant Physiology* **131**, 1868–1876.
- Suchet C., Dormont L., Schatz B., Giurfa M., Simon V., Raynaud C. & Chave J. (2011) Floral scent variation in two *Antirrhinum majus* subspecies influences the choice of naive bumblebees. *Behavioral Ecology and Sociobiology* **65**, 1015–1027.
- Sweetlove L.J., Beard K.F.M., Nunes-Nesi A., Fernie A.R. & Ratcliffe R.G. (2010) Not just a circle: flux modes in the plant TCA cycle. *Trends in Plant Science* **15**, 462–470.
- Szewczyk S., Wolfe E. & Mencer D. (2011) Isolation of the flavor and aroma components of Chinese Five Spice powder. *Abstracts of Papers of the American Chemical Society* **241**, 238-CHED.
- Takeoka G.R., Buttery R.G. & Flath R.A. (1992) Volatile constituents of asian pear (*pyrus-serotina*). *Journal of Agricultural and Food Chemistry* **40**, 1925–1929.
- Tcherkez G., Cornic G., Bligny R., Gout E. & Ghashghaie J. (2005) In vivo respiratory metabolism of illuminated leaves. *Plant Physiology* **138**, 1596–1606.
- Ueda Y., Tsuda A., Bai J.H., Fujishita N. & Chachin K. (1992) Characteristic pattern of aroma ester formation from banana, melon, and strawberry with reference to the substrate-specificity of ester synthetase and alcohol contents in pulp. *Journal of the Japanese Society for Food Science and Technology-Nippon Shokuhin Kagaku Kogaku Kaishi* **39**, 183–187.
- Warneke C., Roberts J.M., Veres P., Gilman J., Kuster W.C., Burling I., Yokelson R. & de Gouw J.A. (2011) VOC identification and inter-comparison from laboratory biomass burning using PTR-MS and PIT-MS. *International Journal of Mass Spectrometry* **303**, 6–14.
- Wegener F., Beyschlag W. & Werner C. (2010) The magnitude of diurnal variation in carbon isotopic composition of leaf dark respired CO₂ correlates with the difference between delta C-13 of leaf and root material. *Functional Plant Biology* **37**, 849–858.
- Wei Y., Lin M., Oliver D.J. & Schnable P.S. (2009) The roles of aldehyde dehydrogenases (ALDHs) in the PDH bypass of Arabidopsis. *BMC Biochemistry* **10**, 7.
- Went F.W. (1960) Blue hazes in the atmosphere. *Nature* **187**, 641–643.
- Werner C., Wegener F., Unger S., Nogues S. & Priault P. (2009) Short-term dynamics of isotopic composition of leaf-respired CO₂ upon darkening: measurements and implications. *Rapid Communications in Mass Spectrometry* **23**, 2428–2438.
- Werner R.A., Buchmann N., Siegwolf R.T.W., Kornel B.E. & Gessler A. (2011) Metabolic fluxes, carbon isotope fractionation and respiration – lessons to be learned from plant biochemistry. *New Phytologist* **191**, 10–15.
- Wieland F., Gloess A.N., Keller M., Wetzel A., Schenker S. & Yeretizian C. (2012) Online monitoring of coffee roasting by proton transfer reaction time-of-flight mass spectrometry (PTR-ToF-MS): towards a real-time process control for a consistent roast profile. *Analytical and Bioanalytical Chemistry* **402**, 2531–2543.
- Xing S.F. & Poirier Y. (2012) The protein acetylome and the regulation of metabolism. *Trends in Plant Science* **17**, 423–430.
- Yani A., Pauly G., Faye M., Salin F. & Gleizes M. (1993) The effect of a long-term water-stress on the metabolism and emission of terpenes of the foliage of cupressus-sempervirens. *Plant Cell and Environment* **16**, 975–981.
- Yokelson R.J., Crouse J.D., DeCarlo P.F., et al. (2009) Emissions from biomass burning in the Yucatan. *Atmospheric Chemistry and Physics* **9**, 5785–5812.
- Zoeller J.R., Agreda V.H., Cook S.L., Lafferty N.L., Polichnowski S.W. & Pond D.M. (1992) Eastman chemical company acetic anhydride process. *Catalysis Today* **13**, 73–91.

Received 25 February 2013; received in revised form 7 July 2013; accepted for publication 8 July 2013

SUPPORTING INFORMATION

Additional Supporting Information may be found in the online version of this article at the publisher's web-site:

Figure S1. Emissions (nmol m⁻² s⁻¹) of MA and ¹³C-MA together with δ¹³CO₂ during a dynamic pulse chase experiment with two detached *H. halimifolium* branches B1 and B2 showing real-time ¹³C-labelling dynamics.

Figure S2. Emissions ($\text{nmol m}^{-2} \text{s}^{-1}$) of MA and ^{13}C -MA together with $\delta^{13}\text{CO}_2$ during a dynamic pulse-chase experiment with two detached *H. halimifolium* branches B3 and B4 showing real-time ^{13}C -labelling dynamics.

Figure S3. Representative time series plots showing diurnal dynamics of oxygenated VOC emissions ($\text{nmol m}^{-2} \text{s}^{-1}$) from an attached *H. halimifolium* branch.

Figure S4. Representative emissions ($\text{nmol m}^{-2} \text{s}^{-1}$) of monoterpenes together with $\delta^{13}\text{CO}_2$ during a dynamic pulse-chase experiment with a single detached *H. halimifolium* branch showing real-time ^{13}C -labelling dynamics at low frequency.

Figure S5. Representative emissions ($\text{nmol m}^{-2} \text{s}^{-1}$) of monoterpenes and the dominant monoterpene fragment together with $\delta^{13}\text{CO}_2$ during a dynamic pulse-chase experiment with a single detached *H. halimifolium* branch showing real-time ^{13}C -labelling dynamics at high frequency.

Figure S6. Representative ^{13}C -labelling dynamics of oxygenated VOCs and CO_2 emissions during dynamic pulse-chase experiments with pyruvate-1- ^{13}C and pyruvate-2- ^{13}C on a single detached *H. halimifolium* branch.